Nanoscale

Accepted Manuscript

This article can be cited before page numbers have been issued, to do this please use: C. T.G. Smith, C. Mills, S. Pani, R. Rhodes, J. Bailey, S. J. Cooper, T. Pathan, V. Stolojan, D. Brett, P. Shearing and S. R. P. Silva, *Nanoscale*, 2019, DOI: 10.1039/C9NR03056E.

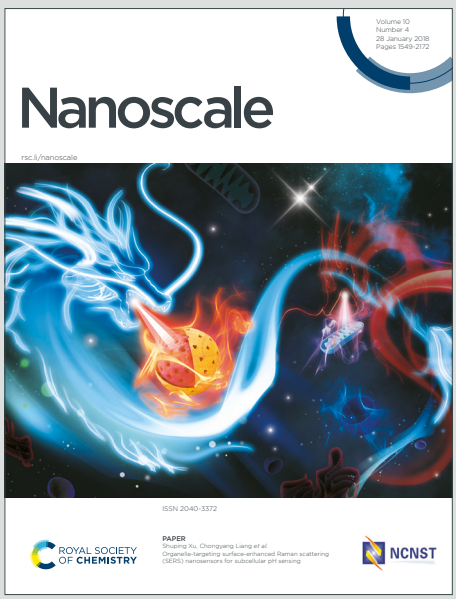

ROYAL SOCIETY OF CHEMISTRY

rsc.li/nanoscale

View Article Online
DOI: 10.1039/C9NR03056E

ARTICLE

X-ray Micro-Computed Tomography as a Non-Destructive Tool for Imaging the Uptake of Metal Nanoparticles by Graphene-Based 3D Carbon Structures

Received 00th January 20xx,
Accepted 00th January 20xx

DOI: 10.1039/x0xx00000x

Christopher T. G. Smith,[a] Christopher A. Mills,[a,b] Silvia Pani,[c] Rhys Rhodes,[a] Josh J. Bailey,[d] Samuel J. Cooper,[e] Tanveerkhan S. Pathan,[d] Vlad Stolojan,[a] Daniel J. L. Brett,[d] Paul R. Shearing [d] and S. Ravi P. Silva [a*]

Graphene-based carbon sponges can be used in different applications in a large number of fields including microelectronics, energy harvesting and storage, antimicrobial activity and environmental remediation. The functionality and scope of their applications can be broadened considerably by the introduction of metallic nanoparticles into the carbon matrix during preparation or post-synthesis. Here, we report on the use of X-ray micro-computed tomography (CT) as a method of imaging graphene sponges after the uptake of metal (silver and iron) nanoparticles. The technique can be used to visualize the inner structure of the graphene sponge in 3D in a non-destructive fashion by providing information on the nanoparticles deposited on the sponge surfaces, both internal and external. Other deposited materials can be imaged in a similar manner providing they return a high enough contrast to the carbon microstructure, which is facilitated by the low atomic mass of carbon.

1 Introduction

The functionalization of three-dimensional (3D) sponge-like nano-carbon materials with metal nanoparticles (NPs) has already been shown to be advantageous for various applications; including energy harvesting and storage,[1] microelectronics,[2] antimicrobial activity[3] and environmental remediation.[4,5] However, examining the microstructure of these structures, in order to get a better understanding of the synthesis and distribution of incorporated nano-structures, has been beset with complications. Methods for imaging the internal structure of these porous nanostructures are limited and typically require extensive, often destructive, sample preparation. In this article, the use of X-ray micro-CT is reported as a method for imaging the uptake of metal NPs into the 3D sponges, potentially allowing for non-destructive imaging of the internal structure of the carbon sponge and accurate determination of the position of the deposited NPs.

X-ray CT methods have been previously identified as a technique suitable for a variety of areas of materials analysis.[6] CT methods find applications in quantitative analysis,[7] materials metrology, and in multimodal studies in combination with other techniques, especially other X-ray modalities such as X-ray diffraction.[8] Applications of CT systems are varied but encompass the non-destructive analysis of inaccessible or fragile samples, and can be utilised to give temporal information. Such applications include: the analysis of materials[9] and biomaterials, such as tooth and bone implants, and medical[10] and biological[11] samples; failure analysis in materials, such as cements, and device components, such as battery electrodes;[12] and the characterisation of matrix materials,[13] amongst others.[14]

Stock[14] has comprehensively listed the areas within materials analysis in which micro-CT methods can be used, including internal material constitution, such as phase distribution, and the analysis of cellular and channel structures. Examples of cellular solids include static, temporally evolving, fibrous networks and mineralised tissues, and biomedical samples. External and processing effects can also be examined, such as deformation, fatigue and fracture in materials, alongside solidification, corrosion and environmental effects. In essence, lab-based X-ray micro-CT operates by acquiring a series of two-dimensional X-ray projection images taken at incremental angles about a central rotation axis that is centred within the area of interest, using the cone-shaped X-ray emission of an X-ray source. These images are subsequently converted to image "slices" using a mathematical algorithm, and the slices are combined to give a 3D reconstruction of the imaged material.

Such imaging is particularly useful for examining cellular structures, and has previously been undertaken on sponge- and

[a] Nano-Electronics Centre, Advanced Technology Institute, University of Surrey, Guildford, GU2 7XH, UK.
[b] Metallic and Functional Coatings Group, Surface Engineering Department, Tata Steel, Research Development and Technology, Talbot building, Swansea University, SA2 8PP, UK.
[c] Centre for Nuclear and Radiation Physics, Department of Physics, University of Surrey, Guildford, Surrey GU2 7XH, UK.
[d] Electrochemical Innovation Laboratory, Department of Chemical Engineering, University College London, Torrington Place, London WC1E 7JE, UK.
[e] Dyson School of Design Engineering, Imperial College London, South Kensington, London, SW7 1NA, UK.
*corresponding author: s.silva@surrey.ac.uk.
Electronic Supplementary Information (ESI) available: [details of any supplementary information available should be included here]. See DOI: 10.1039/x0xx00000x

View Article Online
DOI: 10.1039/C9NR03056E

foam-like materials made of: polymers such as polypropylene, applied to measure displacement fields in cellular materials during impact;[15] metals, such as aluminium, to examine deformation and plastic collapse mechanisms;[16] complex fuel cell materials, as an insight into the interfaces and structural features;[17] and even foods, as an examination of their macro- and micro-cellular structure.[18] Here we examine the use of X-ray micro-CT imaging to examine the uptake of NPs (Fe and Ag) by porous carbon sponges and subsequently use the NP uptake to image the pore structure in the sponge materials. Such a technique has immediate application in the fields of wastewater treatment and environmental remediation, but may also be useful as an *in-vitro* substitute for biological tissue.

2 Experimental

2.1 Reduced graphene oxide sponge preparation

Reduced graphene oxide (rGO) sponges were synthesised according to a previously reported method.[4] In brief, graphite powder (1 g, Fisher Scientific) was added to concentrated sulphuric acid (23 mL, 95% H_2SO_4 Sigma Aldrich) under stirring and cooled to 0 ˚C *via* an ice bath. To this sodium nitrate (0.5 g, Sigma Aldrich) was added, followed by the careful addition of potassium permanganate (3 g, Fisher Chemical). During this step, the rate of addition was adjusted in order to maintain the temperature below 20 ˚C. After addition, the ice bath was removed and the reaction allowed to stir for 30 minutes in ambient conditions, before a subsequent addition of deionised water (46 mL) prompted a sharp increase in temperature to approx. 80 ˚C. After a further 15 minutes, the reaction was terminated through the addition of deionised water (170 mL) and H_2O_2 solution (30% solution, 10 mL, Sigma Aldrich). The precipitate produced was separated and washed repeatedly *via* centrifugation, first with dilute hydrochloric acid (5% solution, Sigma Aldrich) and then with deionised water, before being dried under vacuum at 50 ˚C. Graphite oxide powder (40 mg) was subsequently dispersed via sonication in water (4 mL, 10 mg/mL). An excess of Vitamin C (60 mg, Sigma Aldrich) was then added and sonicated (1 minute, Ultrawave Qi-200) to ensure the Vitamin C was completely dissolved. This solution was then transferred into a glass vial and the carbon sponge produced by heating at 80 ˚C for 2 hours.

2.2 Metal resin preparation

To produce an Fe NP resin, citric acid (0.75 g) was dissolved in water (5 ml), followed by iron (III) nitrate nonahydrate (1 g). Ethylene glycol (7.5 ml) was then added and the resulting mixture was heated to 80 ˚C while stirring. Upon reaching 80 ˚C, the mixture was placed in a bath ultra-sonicator for 30 minutes. This process of heating to 80 ˚C and then sonicating was repeated 3 times.

To synthesise the Ag NP resin, citric acid (0.75 g) was dissolved in water (5 ml), followed by the addition of silver nitrate (200 mg). Ethylene glycol (7.5 ml) was then added and the same heat and sonication treatment applied as with the Fe resin.

2.3 Metal nanoparticle incorporation

To prepare the sponges for X-ray micro-CT analysis, the residual Vitamin C solution surrounding the sponge was carefully decanted, ensuring no agitation to the sponge itself. Metal NP resin (2 ml) was added to the sponge and left to adsorb for 1 hour, before the metal NP resin was carefully decanted (**Figure 1**). To ensure the sponges did not shrink during micro-CT analysis, sponges were freeze-dried prior to CT analysis. Finally, in the case of iron NPs, the sponge was baked at 850 °C for 2 hours under nitrogen to form the NPs. Fragments of the freeze-dried sponges were subsequently examined using a FEI Quanta 200 scanning electron microscope (SEM).

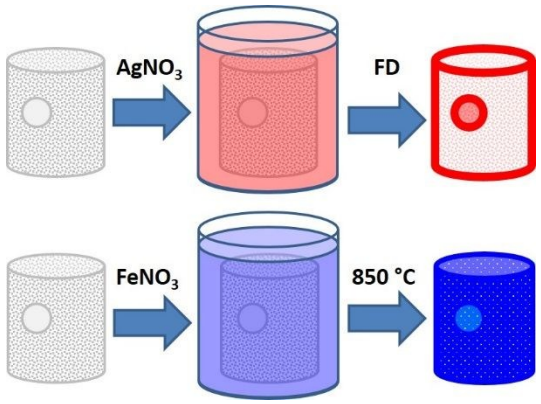

Figure 1 Process diagrams showing the method of integration of (top) Ag and (bottom) Fe NPs into theoretical carbon sponge structures containing one large pore (FD = freeze dry).

2.4 Data acquisition and reconstruction

Micro-CT images were recorded at the Centre for Nuclear and Radiation Physics, Department of Physics, University of Surrey, using an X-ray source with a Molybdenum anode (XTF 5000, Oxford Instruments, UK), a flat panel detector (C7942, Hamamatsu Photonics K.K., Japan) and a caesium iodide (CsI) scintillator. Samples were placed on a translation and rotation stage (Micos VT-80 and DT-80 with a Corvus-eco controller, Micos Engineering GmbH, Switzerland), with a source-sample distance of 90 cm and a source-detector distance of 100 cm. 360 projections were acquired across 180°. Each projection was obtained by summing 20 individual frames, each 0.5 s in duration. The CT slices were then reconstructed with custom-written IDL software based on filtered back-projection with a Shepp-Logan filter.[19] Due to the small sample size compared to the source-sample distance it was sufficient to acquire projections across 180° and to use parallel-beam reconstruction algorithms. Each voxel in this case had equal orthogonal dimensions of 50 µm.

The NP-doped carbon sponges were further examined using a higher magnification laboratory-based X-ray micro-CT instrument (Xradia 520 Versa, Carl Zeiss, CA, USA) available at the Electrochemical Innovation Laboratory, Department of Chemical Engineering, University College London. The scan captured the entire sponge, with an accelerating voltage of 40 kV and an optical magnification of 4×. A pixel size of 4.85 µm

resulted from sample-to-detector and source-to-sample distances which allowed a field-of-view (FOV) that fully captured the sample but maximised detector counts. 1601 projections were acquired at an exposure time of 20 s. These high magnification scans provide greater particulate detail for examination, and allow for more accurate distance mapping.
No binning of the data was used and the 2D projection images were subjected to a filtered back-projection algorithm in order to reconstruct a 3D volume. Image processing, segmentation and subsequent analysis were completed in a 3D visualization and analysis software (Avizo, FEI Visualization Group, France). The scan parameters for X-ray micro-CT are given in **Table 1**, while the segmentation (of the carbon and the NPs) and analysis procedures are detailed in the **supplemental materials** section (see **Supplemental Material)**.

3. Results and Discussion

3.1 SEM analysis

Initially, to confirm the presence of metal NPs inside the sponges, fragments of each sponge were examined using SEM. **Figure 2a** shows a fragment of an rGO sponge that has been submersed in a Ag resin. The magnified image in Figure 2b shows Ag NPs with a range of sizes scattered across a single rGO flake surface. Dimensional analysis shows the particles are approximately 50 – 500 nm in diameter (Figure 2c), which makes them large in comparison to other Ag NPs routinely observed in the literature. The large diameters are due to the high concentration of Ag in the resin. This is preferred to ensure a high concentration of NPs is produced, suitable for increased contrast in the subsequent imaging techniques. This high Ag concentration can however cause NP aggregation as residual vitamin C, present on the sponge surface, further reduces silver nitrate to Ag metal which in turn causes deposited Ag NPs to aggregate with neighbouring particles, creating larger agglomerations. Despite this, while the low magnification SEM image (Figure 2a) shows the porous structure of the rGO sponge material, higher magnification SEM images taken on different areas of the sponge fragment show that the Ag NPs are distributed throughout the entire sponge surface.
In comparison, **Figure 3** shows a sponge left to soak in Fe resin. The SEM images again show a porous structure, similar to the Ag-loaded rGO sponge, however in this case large NPs are not visible. This is because the iron nitrate does not reduce in the presence of any residual vitamin C on the surface of the rGO, instead forming NPs after exposure to elevated temperatures. This allows the resin to uniformly disperse throughout the sponge, without aggregation occurring during NP formation. Figure 3d, which is directly comparable with Figure 2b, shows that no NPs over 50 nm diameter are present.

Table 1 Scan parameters for X-ray micro-CT imaging

View Article Online
DOI: 10.1039/C9NR03056E

Location	Surrey	UCL
Scan	Full	Full
Magnification	1×	4×
Power (kV)	40	40
Pixel size (µm)	50	4.85
Exposure time (s)	10	20
Binning	1	1
Projections	360	1601

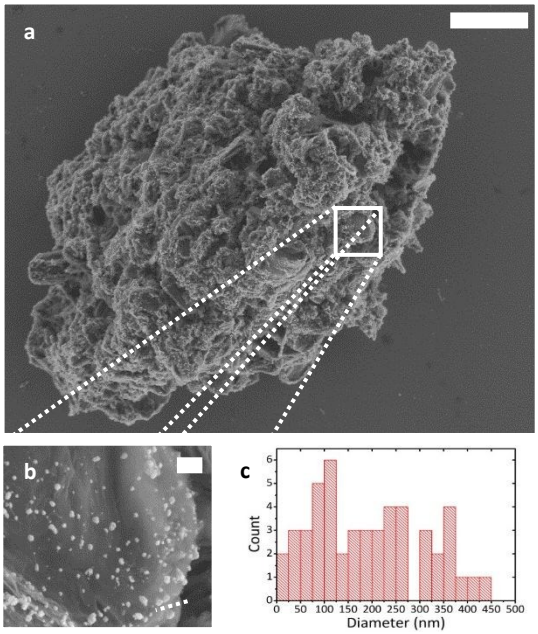

Figure 2 SEM images of a rGO sponge fragment with deposited Ag NPs before freeze-drying [scale bars: (a) 50 µm and (b) 2 µm]. (c) shows the size distribution of the Ag particles measured from (b) (n=52).

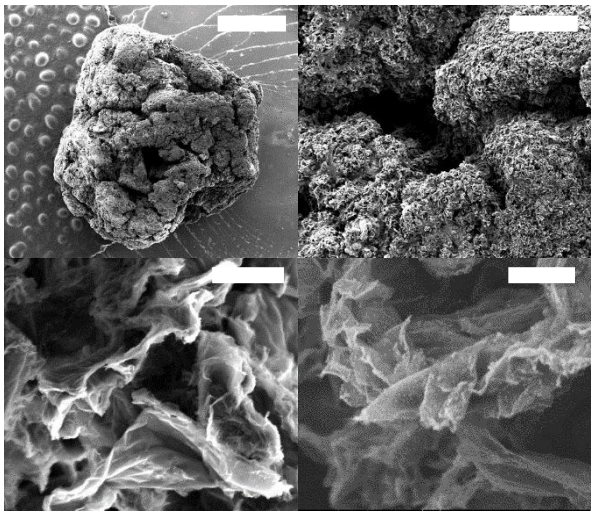

Figure 3 SEM images of an Fe-rGO sponge after thermal treatment [scale bars: (a) 1 mm, (b) 150 µm, (c) 3 µm and (d) 2 µm]. (d) has been brightness and contrast enhanced to allow for discrimination of the NPs on the rGO surface.

3.2 Micro-CT imaging

View Article Online
DOI: 10.1039/C9NR02056E

With the presence of metal NPs adsorbed onto the surface of the rGO sponge confirmed, X-ray CT scanning was used to image the rGO sponges subjected to different concentrations of the metal NP resin. The initial X-ray projections are presented in **Figure 4** which shows a range of Ag NP resin concentrations absorbed into rGO sponges and compares the X-ray projections with a digital photograph. In the X-ray projections a darker colour indicates higher attenuation; the logarithmically scaled image facilitates identification of the pristine sponge and the low concentration NP loaded sponges, even though the image returned is weak for these samples.

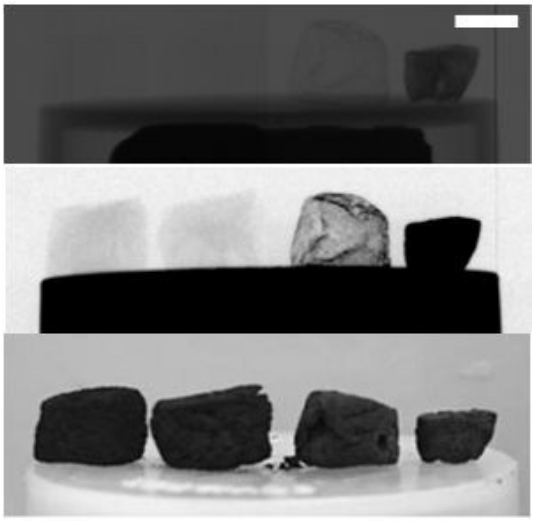

Figure 4 (a) X-ray projection, (b) contrast enhanced logarithmic scaled X-ray image and (c) comparative digital photograph of four rGO_{VC} sponges left to soak in Ag resins of differing concentrations [left to right: 0, 0.2, 2 and 20 mg/mL, respectively] before freeze-drying. [Scale bar: 1 cm]

Using X-ray micro CT, it is possible to reconstruct slices, which can be translated into a 3D representation of the sponge structure. An example of these slices and the corresponding 3D models are presented in **Figure 5** for rGO sponges subjected to two different concentrations of Ag resin (2 and 20 mg/mL). For clarity, the contrast has been arbitrarily scaled to maximise pixel intensities. From the cross-sectional image shown in (c), it can be seen that there is a large amount of Ag built up on the edge of the sponge. It also shows the presence of a large void in the centre of the sponge. There are signs that the Ag has reached the edges of the void, as there is an increase in image intensity around the edges of the void. When taking line profiles across the cross section (**Figure 6**) this amounts to an approx. 1.7× increase in intensity at the edge of the void, when compared to the intensity at the bulk of the sponge. In comparison, the intensity at the outer edge of the sponge is up to a valuable 6.5× more intense. These increases in intensity at the void edges are much clearer in the sponge subjected to the higher concentration of Ag resin (Figure 5f), where the Ag has been absorbed all the way through the sponge, although the intensity increase in this case is only up to 2.7×.

The presence of higher intensity regions around the edges again indicates a possible degree of aggregation of Ag particles at the sponge surface. This is expected as residual vitamin C on the surface of the rGO surrounding the void reduces the silver nitrate to Ag metal NPs which aggregate together to form Ag aggregates. The surface rendering in (e) clearly shows the increased intensity around the voids in the 20 mg/mL Ag resin rGO sponge. From the presence of the Ag coating at the edge of the void, it can be inferred that the void was filled upon addition of the Ag resin. The CT reconstructions of the 20 mg/mL sponge (d – f) clearly show that the Ag has been adsorbed on the surface of the whole sponge and not just the outer surface and that voids are also present in this sponge which are formed when the sponge is produced. We suspect that the aggregation of Ag NPs will eventually affect the subsequent ingress of NPs into the sponge by blocking the outer pores in the sponge surface. However, the relative constancy in NP concentration in the centre of the sponge, as shown in figure 6 (in areas distant from any voids), suggests that the ingress in these sponges is unimpeded, and NP distribution in the sponge innards is uniform.

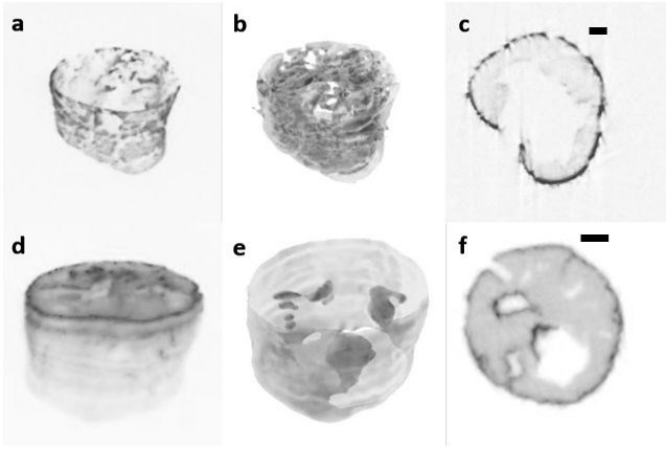

Figure 5 3D models generated from Micro-CT X-ray slices of rGO sponges left to soak in (a – c) 2 mg/mL and (d - f) 20 mg/mL Ag resin. For each image set a 3D model is constructed from the CT data (a and d), surfaces are rendered and smoothed using the highest intensities (b and e) and a cross section is taken (across c and f). Each pixel size is 50 µm, producing a voxel volume of 1.25×10^5 µm^3. For clarity, the contrast has been arbitrarily scaled to maximise pixel intensities. [Scale bars: 2 mm]

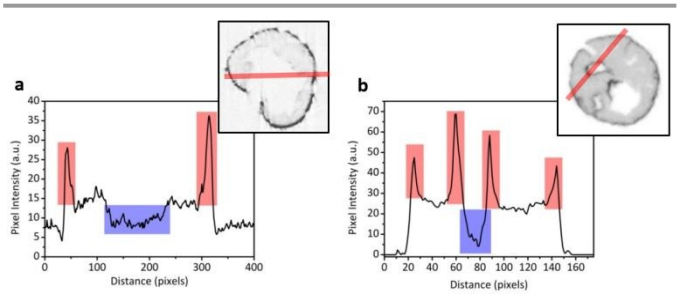

Figure 6 Representative line profiles taken from (a) Figure 5c and (b) Figure 5f. The voids (blue boxes) and areas of high concentration of Ag aggregates (red boxes) are highlighted.

Interestingly, the presence of aggregation at the surfaces of the rGO sponge is not seen when using the Fe resin, as shown in the micro-CT images presented in **Figure 7**. The 3D models in (a) and (b) show that the Fe resin is distributed throughout the whole sponge. Unlike the Ag sponges, the cross section in (c) and the

line profile in (d) show no sharp increase in intensity at the outer surface of the sponge, or around the voids present, thus indicating that Fe NP aggregation does not occur. In contrast, the 3D reconstructions show no signs of aggregation around the edges and pores of the sponge. Rather, a smooth decrease in NP concentration is observed towards the centre of the sponge as shown by the voxel intensity line profile in (e). In this case, the intensity at the edges is approx. 2.2× to 2.7× more intense than that at the centre, but the transition is much less pronounced or obvious than that for the case of Ag.

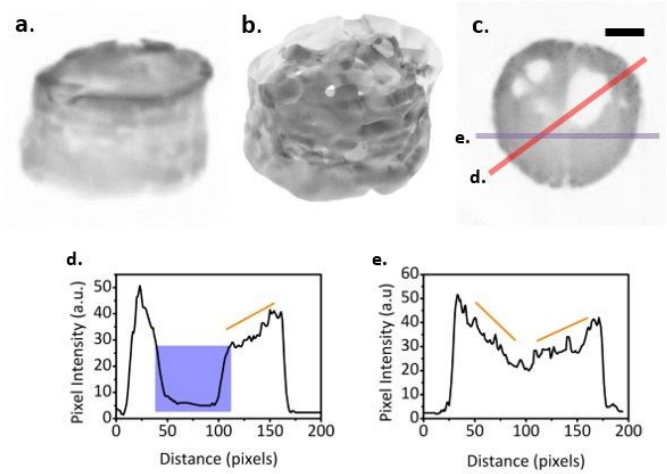

Figure 7 3D models generated from Micro-CT X-ray projections of rGO sponges left to soak in 2 mg/mL Fe resin. For each image set, a 3D model is constructed from the CT data (a), surfaces are rendered and smoothed using the highest intensities (b) and a cross-section is taken (c). (d and e) Representative line profiles taken from (c) show a void (blue box) and the reduction in concentration of deposited Fe NPs (highlighted by the orange lines) upon progressing from the edge of the sponge to the centre. Each pixel size is 50 µm, producing a voxel volume of 1.25×10^5 µm^3. For clarity, the contrast has been arbitrarily scaled to maximise pixel intensities. [Scale bar: 2 mm]

A gradual reduction in intensity from the outside of the sample towards the centre, such as that seen for the Fe-loaded samples (Figure 7) can be indicative of a beam hardening effect, due to the absorption of low energy components at the outer edges. However, the lack of a similar gradual change in intensity in the cross-sections of the higher atomic mass Ag NP-loaded sponges (Figure 6) suggests that the intensity variation in the former may be due to a NP concentration gradient. It may also be that the Fe resin is being adsorbed into the centre of the sponge, depositing Fe NPs on the way, and reducing the concentration of the resin as it moves through the sponge. The higher intensity at the edges of the sponge would therefore suggest that the sponge has not reached maximum capacity, but is instead limited by the concentration of Fe resin available.

3.3 Higher resolution X-ray micro-CT

Higher resolution X-ray micro-CT has been used to further examine the structure of the carbon sponges in greater detail. Initially, a full volume micro-CT grayscale rendering of a Ag-loaded carbon sponge, accounting for as many beam hardening artefacts as possible, was produced (**Figure 8**).
Segmented 2D and 3D images have been compiled from the image giving semi-transparent label volume renderings of the Ag NP-loaded carbon sponges (**Figure 9**). From these images, a quantitative estimation of the surface area and porosity of the sponge has been undertaken using *TauFactor*,[20] an open-source MATLAB-based application, available from[21], for calculating tortuosity factors from tomographic data (see **Supplemental Material** for further details of the analysis), developed at the Electrochemical Science and Engineering Group, Earth Science and Engineering Department, Imperial College London. The quantitative results show that the volume of the carbon in the sponge is approx. 2.2 times the volume of the Ag NPs, while the surface area of the carbon is approx. 2.8 times that of the NPs. The volume-specific surface area (VSSA) of the carbon is approx. 2.9 times that of the Ag NPs [with respect to total solid volume], while the volume-specific interfacial area [carbon-NP] is approx. 1/6 of the total VSSA of carbon (10/61), suggesting a 16 % coverage of the NPs on the carbon sponge. Finally, using a sub-volume of the sponge which omits any macroscopic voids, the estimated porosity of the carbon sponge is 73 ± 3 % (1 standard deviation of error). Given the method of production of the sponges, and the subsequent freeze-drying which will cause them to shrink, approx. 70% porosity appears to be a realistic estimation. In this case, given the structure of the sponge, multiple separate sub-volumes were used to increasing the certainty in the porosity value, but in general a single volume can be entered into *TauFactor* for a similar analysis of a more homogeneous matrix.

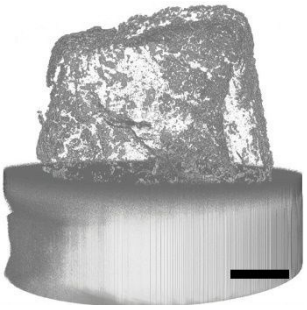

Figure 8 Full volume grayscale rendering of a Ag NP-loaded carbon sponge. Each pixel size is 4.85 µm producing a voxel volume of 114 µm^3. [Scale bar: 2 mm]

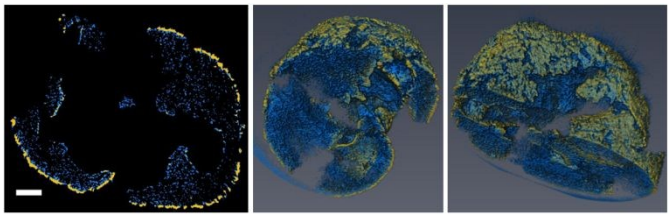

Figure 9 Semi-transparent label volume renderings of the Ag NP loaded carbon sponges (yellow NP, blue carbon). Each pixel size is 4.85 µm, producing a voxel volume of 114 µm^3. [Scale bar: 1mm]

The NP-loaded sponge was further analysed, with respect to the elemental positioning, using *TauFactor*. The matrix in the CT image contains all three phases: pore (0), carbon (1), and Ag NPs (2). Based on their disposition, the "centre-of-mass" (COM) can be located, either separately for a single phase, or for both the carbon and NP phases together. The code then grows a cubic "city block / Manhattan"-based distance matrix (excluding the

View Article Online
DOI: 10.1039/C9NR05056E

diagonals) from the COM. In the final calculation, the programme counts the voxels in each of the growing shells of the distance map and calculates the proportion of each phase of relevance. This ratio is subsequently plotted in **Figure 10**.

View Article Online
DOI: 10.1039/C9NR03056E

ARTICLE

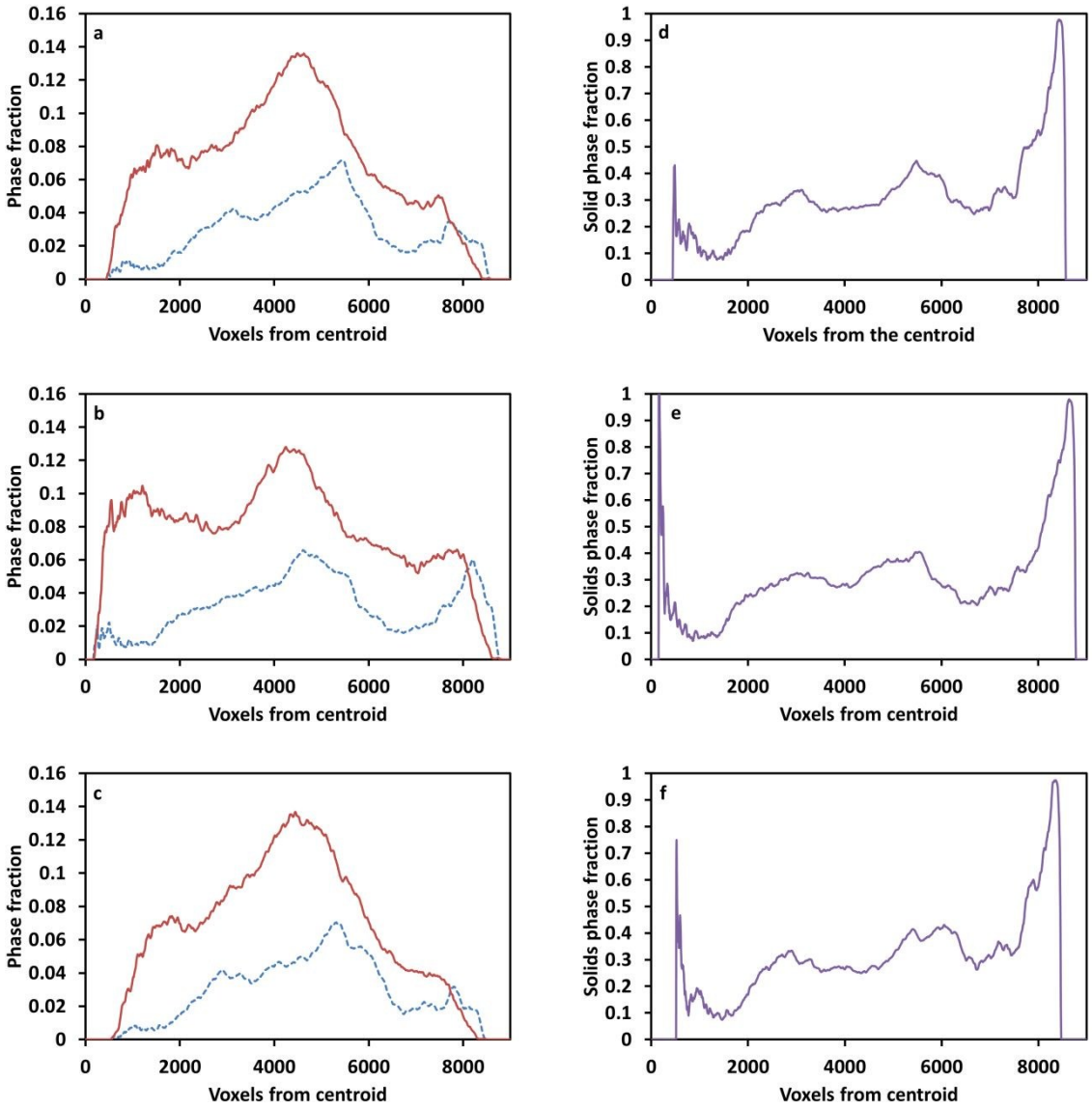

Figure 10 (a-c) Phase fraction of the carbon (solid red line) and Ag NPs (dashed blue line), and (d-f) solid phase fraction ratio (Ag/C), relative to the centre of mass of the carbon sponge X-ray nano CT images, for (a, d) the carbon centroid, (b, e) the Ag centroid, and (c, f) the total solids (Ag + C) centroid (voxel length = 4.85 µm).

In general, in each phase fraction plot, the maximum of the Ag NP curve is offset to the outer side of the carbon, with respect to distance, giving a graphical illustration of the fact that a large number of NPs are positioned on the outer surface of the sponge bulk. This is highlighted by the solid phase fraction ratio (Ag/C) plots, relative to the centre of mass of the carbon sponge, which reveal maxima at the very edge of the sponge surface, furthest from the centroid in each case. In Figure 10c, the maximum carbon fraction can be seen at 4357 voxels (approx. 2.1 mm = number of voxels multiplied by the voxel size [4.85 µm]) from the centroid, whereas for the Ag the maximum is at 5236 voxels (approx. 2.5 mm). Given the irregularity of the outer surface of the sponge, this again suggests that the Ag is most concentrated on the sponge surface.

Figure 10 therefore confirms that there is a greater number of Ag NPs accumulating on the outer surfaces of the sponge than

in the bulk. The detection at this resolution of small numbers of NPs, and with the artefacts inherent in the scan, points to a superficially dependent thresholding during segmentation. However, the corroborating SEM images confirm that there are NPs present, although whether or not they are truly homogeneous is less clear. Figure 10 may suggest this, but it may be that the interior NPs are slightly over-segmented, and further study would be needed to verify this. Our study points to clearly defined limits in the resolution available for 3D rendering of X-ray CT scans, and having multiple imaging techniques allowing for higher confidence in the analysis proposed.

4 Conclusions

In conclusion, it has been shown that X-ray micro-CT is an effective tool for examining metallic NP-decorated rGO based sponges. Examples of rGO sponges decorated with NPs are imaged using the technique, and 3D reconstructions give information on the adsorption of the NPs without destruction of the inner structure of the sample. Even though the diameter of the NPs is shown to be less than the voxel size, the average signal gives an indication of local NP concentrations. Pores present inside the sponge are imaged even by the lower resolution micro-CT apparatus, which suggests that nano-CT apparatus may be able to image the full extent of the sponge's porous structure. Both Ag and Fe NPs are adsorbed onto the surface of the sponge providing contrast for imaging. There is evidence that the Ag NPs agglomerate upon contact with the surface, creating increases in local concentration at the external surface and edges of voids, whereas Fe NPs are shown to distribute more homogeneously across the internal structure of the sponge. Theoretically, a wide range of metal NPs could be used, providing significant contrast is achieved. The possible applications are wide-ranging and not limited to 3D carbon sponges. It is envisioned that the technique could be used to examine the distribution of NPs in applications such as Ag-functionalised carbon water filters, plasmonic NPs in organic photovoltaics, and functional NPs in protective carbon coatings, amongst others. Higher resolution (nano) X-ray CT, in conjunction with a sufficiently small dimensioned NP system, could potentially be able to differentiate between forms of carbon, such as graphitic carbon and carbon nanotubes, by decorating individual molecules.

Conflicts of interest

There are no conflicts of interest to declare.

Acknowledgements

The authors would like to acknowledge funding for this work from DSTL through the provision of a PhD studentship to C. T. G. S. The authors would also like to thank Noel Wardell (Department of Microbial Sciences, University of Surrey) for completing the freeze-drying undertaken in this work.

Notes and references

View Article Online
DOI: 10.1039/C9NR03056E

1 V. Chabot, D. Higgins, A. Yu, X. Xiao, Z. Chen and J. Zhang, *Energy & Environmental Science,* 2014, **7**, 1564-1596.
2 L. Liu, Z. Niu and J. Chen, *Chemical Society Reviews,* 2016, **45**, 4340-4363; Y. Lu and Y. Chen, Chapter 11, Graphene and Porous Nanocarbon Materials for Supercapacitor Applications, in *Nanocarbons for Advanced Energy Storage*, Vol. 1, 2015, X. Feng (Editor), ISBN: 978-3-527-33665-4.
3 N. L. V. Carreño, A. M. Barbosa, V. C. Duarte, C. F. Correa, C. Ferrúa, F. Nedel, S. Peralta, C. A. Mills, R. Rhodes, F. L. M. Sam, and S. R. P. Silva*, Journal of Nanomaterials*, 2017, 6059540
4 E. J. Legge, M. Ahmad, C. T. G. Smith, B. Brennan, C. A. Mills, V. Stolojan, A. J. Pollard and S. R. P. Silva, *RSC Advances*, 2018, **8**, 37540-37549; N. L. V. Carreno M. T. Escote, A. Valentini, L. McCafferty, V. Stolojan, M. Beliatis, C. A. Mills, R. Rhodes, C. T. G. Smith and S. R. P. Silva, *Nanoscale*, 2015, **7**, 17441-17449.
5 X. Zeng, D. T. McCarthy, A. Deletic, and X. Zhang, *Advanced Functional Materials*, 2015, **25**, 4344-4351.
6 L. Salvo, P. Cloetens, E. Maire, S. Zabler, J.J. Blandin, J.Y. Buffiere, W. Ludwig, E. Boller, D. Bellet and C. Josserond, *Nuclear Instruments and Methods in Physics Research Section B: Beam Interactions with Materials and Atoms,* 2003, **200**, 273-286.
7 E. Maireand P. J. Withers, *International Materials Reviews,* 2014, **59**, 1-43.
8 F. A. Dilmanian, Z. Zhong, B. Ren, X. Y. Wu, L. D. Chapman, I. Orion and W. C. Thomlinson, *Physics in Medicine and Biology*, 2000, **45**, 933; D Chapman, W Thomlinson, R E Johnston, D Washburn, E Pisano, N Gmür, Z Zhong, R Menk, F Arfelli and D Sayers, *Physics in Medicine and Biology*, 1997, **42**, 2015.
9 V. Cnudde and M. N. Boone, *Earth-Science Reviews* 2013, **123**, 1-17.
10 A. K. Willi, *Physics in Medicine and Biology*, 2006, **51**, R29.
11 D. W. Holdsworthand M. M. Thornton, *Trends in Biotechnology,* 2002, **20**, S34-S39.
12 D. P. Finegan, M. Scheel, J. B. Robinson, B. Tjaden, I. Hunt, T. J. Mason, J. Millichamp, M. Di Michiel, G. J. Offer, G. Hinds, D. J. L. Brett and P. R. Shearing, *Nature Communications*, 2015, **6**, 6924.
13 A. Elmoutaouakkil, L. Salvo, E. Maire and G. Peix, *Advanced Engineering Materials*, 2002, **4**, 803-807.
14 S. R. Stock, *International Materials Reviews*, 2008, **53**, 129-181.
15 S. Roux, F. Hild, P. Viot and D. Bernard, *Composites Part A: Applied Science and Manufacturing*, 2008, **39**, 1253-1265.
16 I. Jeon, T. Asahina, K.-J. Kang, S. Imand T. J. Lu, *Mechanics of Materials*, 2010, **42**, 227-236.
17 Q. Meyer, J. Hack, N. Mansor, F. Iacoviello, J. J. Bailey, P. R. Shearing and D. J. Brett, *Fuel Cells*, 2019, **19**, 35-42; R. Jervis, M. D. R. Kok, J. Montagut, J. T. Gostick, D. J. L. Brett and P. R. Shearing, *Energy Technology*, 2018, **6**, 2488.
18 K. S. Lim and M. Barigou, *Food Research International*, 2004, **37**, 1001-1012.
19 L. A. Shepp and B. F. Logan, *IEEE Transactions on Nuclear Science*, 1974, **21**, 228-236.
20 S. J. Cooper, A. Bertei, P. R. Shearing, J. A. Kilner and N. P. Brandon, *SoftwareX*, 2016, **5**, 203-210.
21 TauFactor download | SourceForge.net. Available at: https://sourceforge.net/projects/taufactor/. (Accessed: 25th April 2017).

DOI: 10.1039/C9NR03056E

Micro-CT as a Non-Destructive Tool for Imaging the Uptake of Metal Nanoparticles by Graphene Based 3D Carbon Structures

Christopher T. G. Smith[1], Christopher A. Mills[1,2], Silvia Pani[3], Rhys Rhodes[1], Josh J. Bailey[4], Samuel J. Cooper[5], Tanveerkhan S. Pathan[4], Vlad Stolojan[1], Paul Shearing[4] and S. Ravi P. Silva[1*]

Table of contents figure

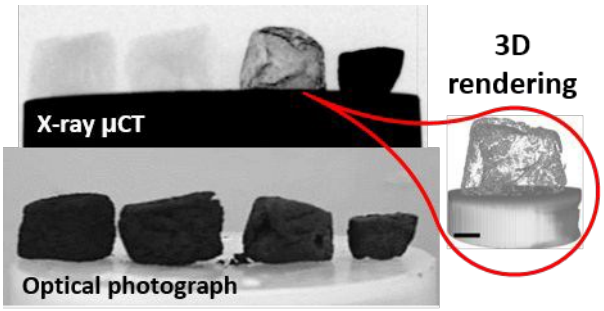

Showcasing X-ray micro-computerized tomography as a method to image metal nanoparticle dispersion throughout sponge-like graphene matrices suitable for environmental remediation